Title:

Computational IR – spectroscopy of interfacial water at fluorinated and non-fluorinated hydrophobic surfaces

Author(s):

Maximilian R. Becker, Roland R. Netz

Computational IR – spectroscopy of interfacial water at fluorinated and non-fluorinated hydrophobic surfaces

Maximilian R. Becker, Roland R. Netz

April 14, 2022

Abstract We report ab-initio simulations of the interface between water and fluorinated and non-fluorinated hydrocarbon self assembled monolayers (SAMs) and compare with the prototypical interfacial system, the vapor-water interface. The thickness of the microscopic depletion layer between SAMs and water is larger for the fluorinated SAM, consistent with the larger contact angle of fluorinated SAMs. We calculate the infrared absorption spectrum of interfacial water, which displays a prominent sharp peak at around 3700 cm^{-1}, signaling the presence of dangling OH bonds. We describe the vibrational properties of dangling OH bonds by a harmonic model and show that spectral line shifts reflect OH-dangling-bond interactions with the surface and line widths report on the rotational lifetimes of dangling OH configurations.

1 Introduction

Adsorption of fluorinated amphiphiles on metal substrates has provided a tool to modify surfaces with a broad range of technological applications in nanotechnology like fabrication of thin film transistors,[1] protection and functionalization of nanostructures,[2,3] creation of nanoelectronics[4] and microelectromechanical systems.[5] Many of these applications make use of the change of physical properties of generated films upon including fluorocarbon segments, in particular friction and wettability properties,[6,7] as they are known to enhance the hydrophobicity as well as the oleophobicity. Self-assembled monolayers of fluorinated alkanethiols (FSAMs) adsorbed on various metal substrates are a widely used and easily controlled platform to study fluorinated thin films. Comparison with their unfluorinated counterparts (HSAMs) has revealed larger contact angles of FSAMs for various liquids,[8,9] while still providing higher thermal stability[10] and higher chemical and biological inertness.

For individual fluorinated molecules solvated in aqueous solution, it has been established that the main driving force of hydrophobicity is the large amount of work needed for forming a fluor-sized cavity, which counteracts the electrostatic binding affinity between water molecules and the polar C-F bond.[11] Recently, it has been shown that a similar effect is the reason why perfluorinated self assembled monolayers (SAMs) exhibit larger hydrophobicity than their non-fluorinated counterparts.[12] It was shown that the dominant interactions between nonpolar SAMs and water are dispersive interactions, which are proportional to the grafting density of the SAMs. Because of the inherent size of fluor molecules as well as the helicity of perfluorinated linear hydrocarbons, the grafting density of perfluorinated SAMs is considerably lower than of the corresponding non-fluorinated molecules - thus the strongly hydrophobic behavior. However, the available theoretical studies on the hydrophobicity of fluorinated surfaces are mostly performed with empirical force-fields, which are designed to reproduce certain macroscopic properties, like contact angles or friction coefficients, but still have several shortcomings and miss out on fundamental physical processes which are of special importance at interfaces. For example, it is known that water molecules change their dipole moment from 1.85 D in vacuum[13] to 2.9 D[14] in the liquid phase, an effect that is clearly missed in non-polarizable force-field models. Likewise, spectroscopy becomes more and more the prime experimental tool to study interfacial properties and is difficult to address with empirical force fields.

Here, we report a large scale study of perfluorinated and non-fluorinated SAMs in contact with a water slab from ab-initio simulations. We show that the microscopic water structure compares well with results from empirical force fields and that key quantities, like the thickness of the microscopic depletion layer, are consistent with experimental and previous computational predictions. We compare the microscopic water structure to the prototypical hydrophobic interface, the vapor-liquid water interface. The first interfacial water layer of all these interfaces is mostly comprised of water molecules whose hydrogen bond network is perturbed and one of the OH - bonds freely "dangles" towards the interface. Such free OH bonds, which are sticking out of the water into the microscopic depletion layer, are accessible to experimental measurements like second harmonic generation[15] or sum frequency generation[16–18] and have been used as a microscopic measure for the hydrophobicity of molecules[19,20] and surfaces.[21] We perform a detailed analysis of the spectral properties of the dangling OH-bond peaks in terms of their amplitude, position and line shape and correlate these spectral properties with the interactions between surfaces and the interfacial water.

2 Results and Discussion

2.1 Structure of interfacial water

We conduct equilibrium simulations of three hydrophobic interfaces employing BLYP-D3 density-functional molecular dynamics (DFT-MD) and corresponding simulations using empirical force-field molecular dynamics (FF-MD). The systems we are analyzing are shown in Fig. 1A: i) The neat vapor – water interface as a reference state for a hydrophobic interface with a 180° contact angle. ii) A self-assembled monolayer

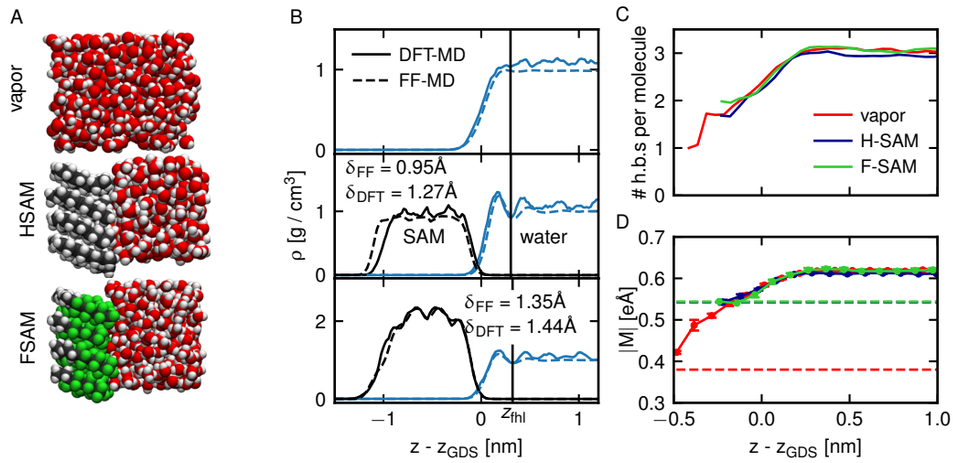

Figure 1: Interfacial water structures at hydrophobic surfaces. A: Simulation snapshots from DFT-MD simulations of the three different considered systems: The vapor-liquid water interface, a water slab in contact with a SAM consisting of octane molecules, a water slab in contact with a SAM consisting of H2F6 molecules. B: Corresponding density profiles from DFT-MD and FF-MD simulations. C: Profiles of the number of hydrogen bonds per water molecule from DFT-MD. D: Profiles of the average dipole moment per water molecule from DFT-MD. The red line denotes the average polarization of single water molecule in the vapor phase. The green and blue broken lines denote the polarization of interfacial water molecules.

consisting of n-Octane CH_3–$(CH_2)_6$–(CH_3) molecules in contact with water (HSAM) and iii) a self assembled monolayer of fluorinated n-Octane molecules CH_3–CH_2–$(CF_2)_5$–(CF_3) (FSAM).

We compare DFT-MD simulations to FF-MD simulations based on the OPLS-AA force-field,[22] which was recently reparametrized to predict the contact angles of water droplets of very similar SAMs.[12] The equilibrated density profiles are shown in Fig. 1B. It is seen that the density profiles from DFT-MD and FF-MD agree well. In particular the width and height of the first hydration layer agree nicely, which indicates good agreement of the interfacial-water structure between the simulation techniques. The standard way to quantify the interaction energies between liquids and solids, the measurement of the contact angle, is computationally not feasible with DFT-MD, due to the need of averaging over extremely long trajectories. But it is known, that the thickness of the microscopic depletion layer between a surface and water is strongly correlated to the contact angle[23] and can be used as a proxy, which can be converged with considerably less statistics. We calculate the thickness of the depletion layer according to

$$\delta = \int_{z_s}^{z_l} \left(1 - \frac{\rho_s(z)}{\rho_s^{\text{bulk}}} - \frac{\rho_l(z)}{\rho_l^{\text{bulk}}}\right) \mathrm{d}z \,. \tag{1}$$

The calculated depletion thicknesses, which are depicted in Fig. 1, agree qualitatively between DFT-MD and FF-MD. Both predict a higher hydrophobicity of FSAMs with respect to HSAMs. The slight increase of the depletion layer thickness from DFT-MD to FF-MD presumably is due to multiple reasons: To speed-up our DFT simulations, we employ a reduced dispersion correction cut-off of 7Å, which will reduce the interfacial interaction energy. On the other hand, DFT-MD takes polarization effects of water molecules into account, while the SPC/E water model is not polarizable and is parametrized to reproduce bulk properties. This could lead to a slight overestimation of electrostatic interactions between water and the SAMs in FF-MD simulations. The mean dipole moment per water molecule as a function of the position from the interface from DFT-MD is displayed in Fig. 1D. While the dipole moment of water increases by more than 50% from vapor to the bulk phase, this is not true for the SAM – water interfaces. The water dipole moment is strongly correlated to the mean number of hydrogen bonds each molecule is participating in. The hydrogen-bond number profile, employing the standard hydrogen bond definition[24] O – O distance $>$ 3.5Å and O – H – O angle $>$ 150°, is shown in Fig. 1C. SAM – water interfaces are less diffuse than the vapor – water interface. While for the vapor – water interface molecules closest to the vapor phase are only very weekly hydrogen bonded (the red line in Fig. 1C ends at 1 hydrogen bond per molecule), molecules in direct contact with the SAM remain significantly hydrogen-bonded (the blue and green lines end at roughly 2 hydrogen bonds per molecule). This leads to a significant polarization of water molecules close to SAMs. Moreover, the polarization profiles in Fig 1D reveal that, while the profiles are nearly identical for all three interfaces far from the interface, very close to the SAMs, the polarization shows a short plateau and deviates from the vapor-water interface. This plateau indicates a polarization of water molecules induced by the SAMs themselves. The fact that the polarization of water molecules in direct contact with SAMs deviates substantially less from bulk water polarization then for the vapor-water interface presumably explains why non-polarizable FF water models are able to reproduce the properties of SAM-water interfaces rather well.

While the main governing energetics of the SAM's hydrophobicity have been subject to studies with empirical force fields,[12] the underlying microscopic interactions of the interfacial water with the surface remain unclear. In order to elucidate the microscopic interaction between the interfacial water and the interfaces, we analyze the orientational distribution of OH bonds as a function of the position of water molecules. In Fig. 2 we show the conditional probability that an OH bond forms an angle θ with the interface given the center of mass of the water molecule it belongs to is at position z. Here, an angle of 180° refers to a bond which points out of the water towards the interface and an angle of 0° to a bond which

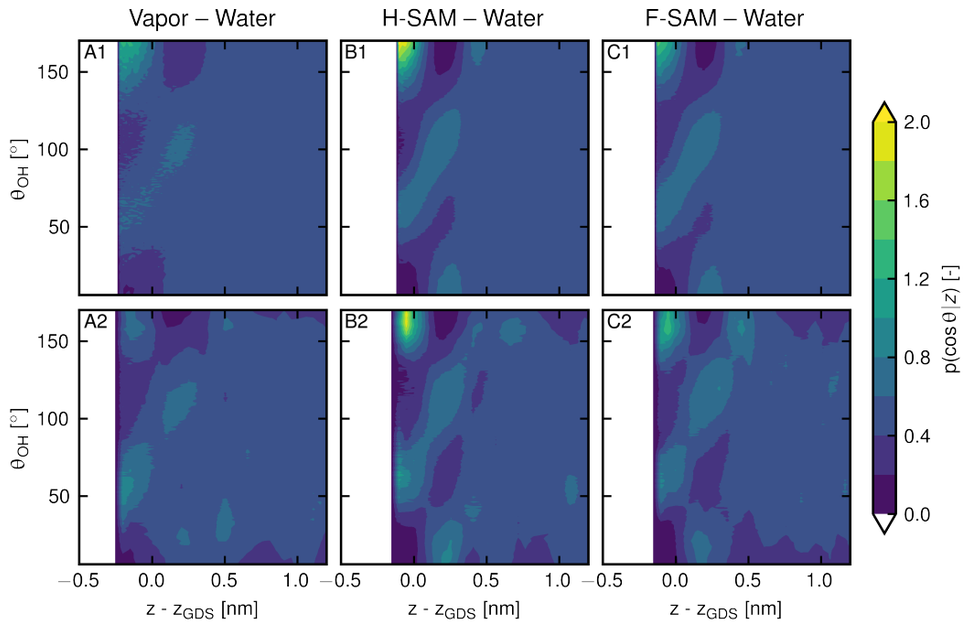

Figure 2: Probability distributions of OH-bond angles for water molecules at position z. In the upper row results from FF-MD simulations are shown, in the lower row DFT-MD results.

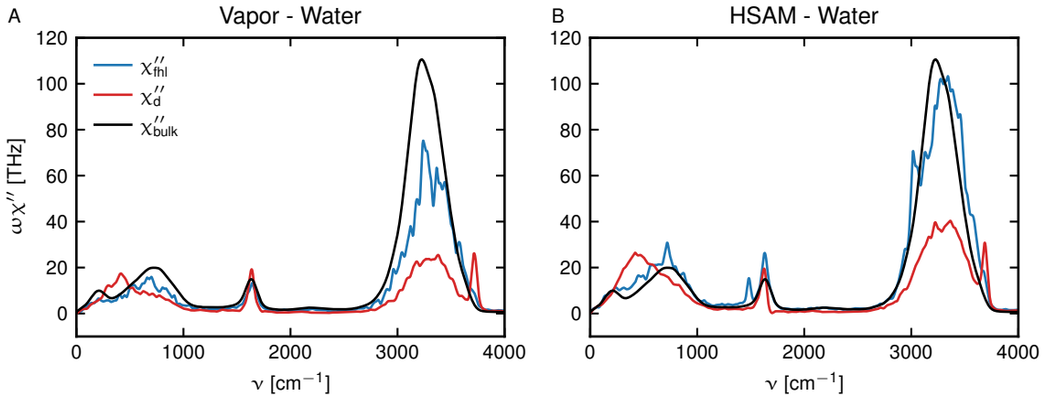

Figure 3: Infrared absorption spectra of interfacial water. A: IR spectrum from the first hydration layer of the vapor water interface compared to the contribution from water molecules containing a dangling OH-bond. The black solid line shows the absorption spectrum of bulk liquid water[27] All absorptions spectra a normalized with respect to the according number of water molecules used to calclate the spectrum. B: Contributions from water molecules in the first hydration layer and n-octane molecules in the SAM compared to contributions from water molecules containing a dangling OH - bond.

points towards the water phase. The main structural feature common to all displayed hydrophobic interfaces is a strong orientation of the outermost layer of water molecules ($z - z_{\mathrm{GDS}} < 0$ nm) with one bond pointing straight out of the water phase towards the interface with $\theta \approx 180°$; therefore the second bond is restricted to an angle of $\theta \approx 75°$. This configuration of water molecules is known in literature as free or dangling OH bonds. The second layer of water molecules ($z - z_{\mathrm{GDS}} \approx 0.2\,\mathrm{nm}$) orients into the opposite direction with one bond pointing towards the water phase at $\theta \approx 0°$. In contrast to FF results, DFT-MD predicts that dangling water molecules orient not straightly towards the interface but they form a $\theta \approx 165°$ angle with it which is consistent with experimental values from the literature.[15] For the vapor – water interface recent theoretical and experimental results indicate even smaller average angles of free OH groups[25]

2.2 IR spectroscopy of first hydration layer

The behavior of dangling OH bonds is of particular importance for the characterization of the interaction of interfacial water with different surfaces. Since the dangling OH is in direct contact with a surface, its behavior can be used to study the properties of the surface itself. Dangling water structures at the vapor-water interface have been studied experimentally using SFG measurements and theoretically with DFT-MD and FF-MD[25,26] methods. In principal, surface specific absorption spectroscopy techniques, like surface enhanced infrared absorption spectroscopy (SEIRAS), are capable to capture signals from dangling OH bonds.

The infrared absorption spectrum of a spatially homogeneous system can be calculated according to

$$I(\omega) \propto \omega\tilde{\chi}''(\omega) = \frac{\omega^2}{2k_B T}\tilde{C}_{MM}(\omega) \tag{2}$$

where $\tilde{C}_{MM}(\omega)$ denotes the Fourier transformation of the dipole-dipole autocorrelation function $C_{MM}(t) =$

$\langle \mathbf{M}(0) \cdot \mathbf{M}(t) \rangle$ of the dipole moment $\mathbf{M}$ of a system. Since in the systems under study, only a small fraction of water molecules is in the dangling configuration, we calculate the absorption spectrum of only the first hydration layer, defined by the position of the first minimum of the density profiles in Fig. 1B at $z \approx z_{\mathrm{GDS}} + 3\text{Å}$. The contribution of the first hydration layer to the absorption spectrum is given by

$$\omega \tilde{\chi}''_{\mathrm{fhl}}(\omega) = \frac{\omega^2}{2k_B T} \int_{-\infty}^{\infty} \left[\langle \mathbf{M}_{\mathrm{fhl}}(0) \cdot \mathbf{M}(t) - \langle \mathbf{M}_{\mathrm{fhl}} \rangle \langle \mathbf{M} \rangle \rangle \right] e^{i\omega t} \mathrm{d}t \,, \tag{3}$$

with the polarization of the first hydration layer $\mathbf{M}_{\mathrm{fhl}}$ and of the total system $\mathbf{M}$ (see appendix). The second term subtracts the nonzero average polarization of water molecules in the first hydration layer. The resulting absorption spectra of the vapor-water system and the HSAM – water system are shown in Fig. 3. In order to calculate the dipole moment of the first hydration layer a spatial decomposition of the electronic density is needed. We use maximally localized Wannier functions to calculate the molecular dipole moments and from that calculate the dipole moment of all water molecules in the first hydration layer. This decomposition is computationally not feasible in case of perfluorinated carbohydrates, such that we do not show results for the FSAM – water system. The absorption spectra of the first hydration layer are overall quite similar to the bulk water spectrum. The vapor – water spectrum has a decreased intensity, in particular of the OH-stretch region around 3300 cm^{-1} and in the librational region around 660 cm^{-1}. This is mainly due to an overall reduced dipole moment of water molecules, as can be seen from Fig. 4D. In the HSAM – water spectra additionally the C-H stretch peak at 3018 cm^{-1} and the C-H bend peak at 1480 cm^{-1} appear, which are originating from the HSAM.

In both spectra there is no clear evidence of dangling water vibrations seen. Therefore, we develop a geometric criterium to define dangling OH bonds, based on the position z_{COM} of the water molecule to which the bond belongs and the angle θ_{OH} the bonds forms with the interface. A detailed explanation is found in the appendix. Recently, similar criteria for dangling bonds have been developed for the vapor-water case, based on computational SFG spectra.[26] There, the hydrogen bond state of molecules in the vicinity of the interface is used to define dangling water.

Based on the definition for dangling water molecules, we calculate the IR absorption contribution of dangling water according to

$$\omega \tilde{\chi}''_{\mathrm{d}}(\omega) = \sum_{i}^{n_{\mathrm{H_2O}}} \frac{\omega^2}{2k_B T} \int_{-\infty}^{\infty} \left[\langle \mathbf{M}_i^{\mathrm{d}}(0) \cdot \mathbf{M}_i(t) \rangle - \langle \mathbf{M}_i^{\mathrm{d}} \rangle \cdot \langle \mathbf{M}_i \rangle \right] e^{i\omega t} \mathrm{d}t \,, \tag{4}$$

with

$$\mathbf{M}_i^{\mathrm{d/nd}}(t) = \begin{cases} \mathbf{M}_i^{\mathrm{d/nd}}(t) = \mathbf{M}_i(t) & \text{if molecule } i \text{ contains a dangling / nondangling bond} \\ 0 & \text{otherwise .} \end{cases} \tag{5}$$

The resulting contributions from dangling water molecules to the spectrum of the first hydration layer are shown in Fig. 3. Because the contribution is very small, we normalized the dangling contribution to the number of dangling water molecules. In the OH - stretch region one can clearly distinguish a narrow peak at 3715 cm^{-1} (vapor) and 3687 cm^{-1} (HSAM) which corresponds to the vibration of the dangling bond and a broader peak around 3300 cm^{-1} which corresponds to the hydrogen bonded second OH - bond. The overall intensity of the contribution of the dangling OH bond is very small compared to the nondangling counterparts in the first hydration layer. This has two reasons: The overall absorption spectrum can be decomposed into a collective and a single molecular contribution,[27] as shown in appendix Sec. A.2. There is a strong collective contribution in the OH - stretch region stemming from correlated polarizations of hydrogen-bonded OH bonds. Since dangling OH bonds are not hydrogen bonded, the collective contribution is reduced. Secondly, hydrogen-bonded water molecules are more strongly polarized than free water molecules, which increases their absorption, compare appendix Sec. A.2, where we predict a 3.3 times larger IR activity of bulk phase OH bonds compared to vapor phase OH - bonds.

2.3 Vibrational analysis of dangling water

In order to analyze the dynamics and energetics of dangling OH - bonds, it is convenient to change from a dipole-moment-based description to a core-position-based description of absorption spectroscopy. Since the dipole moment of a single water molecule is to first order proportional to its OH - bond distances, the IR absorption spectrum in the OH - stretch region can be described by

$$\omega \tilde{\chi}''(\omega) \propto \frac{\omega^2}{2k_B T} \tilde{C}_{dd}(\omega), \tag{6}$$

where $\tilde{C}_{dd}(\omega)$ is the Fourier transform of the OH distance autocorrelation function (see appendix Sec. A.2 for more details). Similar coordinates have recently been used to analyze the frequency-dependent friction of OH-stretch and bend vibrational modes in bulk water.[28] Here we model the dangling OH bond as a damped oscillator in a non harmonic potential,

$$m_{\mathrm{eff}} \ddot{d}_{\mathrm{OH}}(t) = -\gamma \dot{d}_{\mathrm{OH}}(t) - \nabla U(d_{\mathrm{OH}}), \tag{7}$$

with effective mass m_{eff}, constant friction coefficient γ and effective potential U.

In Fig. 4A we show the velocity autocorrelation spectrum of the OH distances of all water molecules in the first hydration layer of the three analyzed interfaces. In contrast to the dielectric absorption spectra

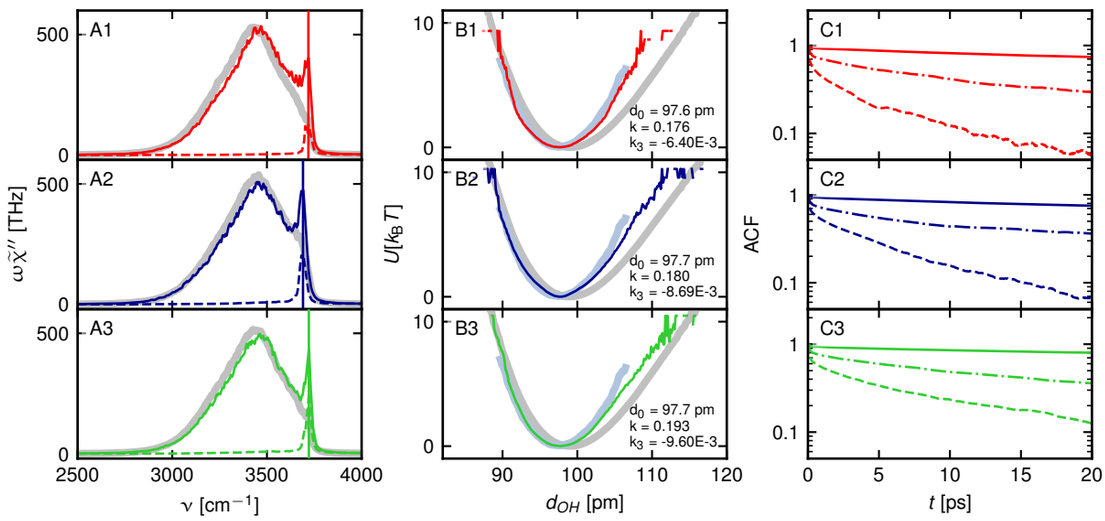

Figure 4: Properties of dangling OH bonds at the three different interfaces. 1st row vapor-water, 2nd row HSAM-water, 3rd row FSAM-water. A: Velocity autocorrelation of OH-bond lengths in the first hydration shell (colored solid lines) and the contributions of dangling OH bonds (colored dashed lines) normalized with respect to the number of water molecules in the first hydration shell. The thick grey line shows the spectrum of all water molecules. B: Effective potential of dangling OH bonds (solid colored line) compared to the effective potential of all OH bonds (grey lines) and of water molecules in vapor phase (light blue lines). C: Configurational autocorrelation functions (see text for details) of water molecules in the first hydration layer (solid lines), water molecules at dangling distance (dashdotted lines) and water molecules which have at least one dangling bond (dashed lines).

shown in Fig. 3, there are pronounced dangling-water peaks visible around 3700cm^{-1}. The difference of the dangling OH-bond signature in the dipole and bond-length autocorrelations is expected due to the low dipolar response of dangling OH bonds. From the spectra we determine the dangling-water peak positions as 3718.9cm^{-1}, 3690.4cm^{-1} and 3721.5cm^{-1} for the vapor-water, the HSAM-water and the FSAM-water interface, respectively.

By employing the criterion for dangling OH bonds we introduced earlier, we calculate the contribution of dangling OH bonds to the spectrum of the first hydration layer. It separates nicely from the broad bulk water peak and explains nearly the full amplitude of the peak, indicating good predictive power of the dangling bond criterion. The area below the dangling contribution of the spectra is proportional to the average number of dangling water molecules, which we determine to be 0.75/nm^2, 1.67/nm^2 and 1.55/nm^2 for the vapor – water, the HSAM – water and the FSAM – water systems. We find a higher proportion of dangling water molecules in the first hydration layer of the HSAM compared to its fluorinated counterpart. This is surprising, since one would assume that water hydrogens, which have a positive partial charge, show stronger affinity towards fluor atoms, which are highly electronegative. This also stands in contrast to previous findings, according to which one can find considerably more dangling OH bonds in the hydration shell of single fluorinated solutes than of unfluorinated solutes.[29] Indeed, further analysis of the dangling bond vibrations substantiates our finding. We determine the effective potential in Eq. 7

$$U(d) = -k_{\mathrm{B}}T \log(P(d)) \tag{8}$$

from the probability density P of a dangling OH bond to assume the length d. In Fig. 4B we show the effective potentials of dangling bonds and compare them to the effective bond potentials of molecules in bulk water as well as in the vapor phase.

We fit the dangling bond effective potential to an anharmonic polynomial model

$$U(d) = \frac{k}{2}(d-d_0)^2 + \frac{k_3}{3}(d-d_0)^3\,. \tag{9}$$

The raw fits are shown in the appendix. In bulk water it was shown that frequency dependent friction in combination with an anharmonic potential is very important in order to determine the correct lineshape and position of the OH stretch peak.[28] This does not hold true for the dangling bond vibrations we are investigating. Assuming a harmonic oscillator with spring constants taken from the fits according to Eq. 9 (spring constants are depicted in Fig. 4B) and effective masses calculated from the equipartition theorem ($m_{\mathrm{eff}}^{vapor} = 0.898$ a.m.u, $m_{\mathrm{eff}}^{HSAM} = 0.973$ a.m.u, $m_{\mathrm{eff}}^{FSAM} = 0.996$ a.m.u,), we predict 3691 cm^{-1}, 3604 cm^{-1} and 3708 cm^{-1} for the vapor - water, HSAM – water and FSAM water systems. The oscillation frequencies of dangling water molecules at the vapor – water and the FSAM – water interface are matched nearly perfectly while the HSAM – water frequency is slightly underestimated (compare vertical lines in Fig. 4A). This indicates that the effective potentials in Fig. 4B do predict the dangling bond vibrations. We conclude that spectral line shifts between different interfaces are of energetic origin and are due to a slightly attractive interaction of the FSAM with OH-bonds, while the contact to the HSAM softens the potential compared to the vapor water interface, which is consistent with experimental results.[18]

The velocity power spectrum of the linearized equation of motion in Eq. 7 is given by a Lorentzian

$$\omega\tilde{\chi}''(\omega) = \frac{\omega^2\gamma}{(k - m_{\mathrm{eff}}\omega^2)^2 + \gamma^2\omega^2}\,. \tag{10}$$

Fitting the dangling OH peaks with this Lorentzian line shape, we find the full width at half maximum (FWHM) to be $\frac{\gamma}{m_{\text{eff}}} = 28.9$ cm^{-1} (vapor), 37.2 cm^{-1} (HSAM) and 38.3 cm^{-1} (FSAM). In the appendix we show that the Lorentzian lineshape describes the data well. The width of the Lorentzian fits defines vibrational lifetimes, which qualitatively match lifetimes we calculate for different configuration of water molecules in the interfacial region depicted in Fig. 4C. We show configurational autocorrelation functions by assigning a state 1 or 0 to every molecule at every time t, depending on whether the molecule is in a certain state or not. Analyzed states are: i) a molecule is in the first hydration layer, ii) a bond is in the dangling distance from the interface but has a random angle to the interface, and iii) an OH bond is in the dangling configuration (both distance and angle match). All autocorrelation functions are characterized by a fast initial decay followed by an exponential regime. Since the relaxation from the dangling state is clearly non-exponential, a direct quantitative comparison with the Lorentzian fits is not possible. The overall trend on the other hand is similar. The vapor water and HSAM- water systems display very similar line widths and dangling lifetimes, while the dangling configuration at the FSAM decays more slowly, corresponding to a narrower peak. From the partitioning into configurations which match both dangling criteria and a state which only matches the right distance of water molecules to the interface, the nature of stabilization of dangling OH bonds at the FSAM is apparent. While at the vapor - water and the HSAM water interface the lifetime of dangling OH bonds is determined in equal proportions by water molecules leaving the outermost layer in z-direction and water molecules rotating out of the dangling state, the angular reorientation of dangling OH bonds is strongly stabilized, which supports the idea of an energetically non favorable H-F interaction.

3 Conclusion

DFT-MD simulations of HSAM-water and FSAM-water interfaces are used to analyze the interfacial water structures and the spectroscopic signatures of interfacial water. We find a larger thickness of the depletion layer in the fluorinated case, consistent with the higher hydrophobicity of FSAMs compared to HSAMs. Analyzing the dynamics of freely dangling OH bonds, a detailed picture of the interfacial water energetics and dynamics at these different surfaces emerges. We show that the dangling OH-bond dynamics can be described by a simple harmonic model with constant friction. This allows for an interpretation of spectral line shifts in terms of the interaction of interfacial water molecules with the surface. In general, we find a larger population of dangling OH bonds for non-fluorinated interfaces, opposite to what is found for fluorinated molecular solutes in bulk water. On the other hand, the lifetime of dangling OH-bonds in the first hydration layer of fluorinated SAMs is strongly increased. This is due to a slow down of the rotational motion of dangling OH bonds at FSAMs compared to HSAMs and at HSAMs compared to the vapor-water interface. The slight blue shift of the dangling OH frequency at FSAMs with respect to the vapor-water interface indicates an energetically favorable interaction and is contrast by a red shift at HSAMs.

4 Acknowledgements

We acknowledge support by Deutsche Forschungsgemeinschaft, Grant CRC 1349, code 387284271, Project C04.

5 Methods

MD - Simulations All DFT-MD simulations are performed with the CP2K 6.1 software package using a contracted double-ζ basis set for valence electrons with GTH pseudopotentials (DZVP-MOLOPT-SR-GTH), the BLYP exchange-correlation functional and the D3 dispersion correction.[30–32] CP2K employs a dual space representation of the electronic densities. We use a 400 Ry cut-off for the plane-wave representation. In our simulations we use a 0.5 fs timestep and control the temperature with the CSVR thermostat at a time constant of 500 fs to a target temperature of 300K.

Molecular dipole moments are obtained from the charge centers of maximally localized Wannier functions at a time resolution of 4 fs for the vapor - water and HSAM - water systems and at a resolution of 50 fs for the FSAM - water system. A charge of -2e is assigned to each charge center, which results together with core charges reduced by electronic charges of the inner shell to molecular dipole moments. Vibrational spectra are smoothed using a Gaussian kernel with 10 cm^{-1} width.

FF-MD simulations are performed with the GROMACS/2020.7 software suite.[33] We use an OPLS/AA[34] based force-field for partially fluorinated hydrocarbons, which has recently been reparametrized by our group to better represent dihedrals in SAMs.[12] For unfluorinated hydrocarbons we use standard OPLS/AA parameters. We employ 2.0 fs time steps and the CSVR thermostat with 1.0 ps time constant.

Vapor – Water System The vapor – water systems shown in Fig. 1A contains 352 water molecules in a periodic box of the size 2 nm x 2 nm 6 nm. For DFT-MD simulations we equilibrate the system from a FF-preequilibrated structure for 15 ps and conduct a production run for 95 ps. The FF-MD vapor water interface was equilibrated for 1 ns with successive 10 ns production run.

SAM Systems We simulate 16 (partially fluorinated) hydrocarbons with 198 (HSAM) and 286 (FSAM) water molecules in DFT-MD and 200 hydrocarbons in two layers between which there are 2089 (HSAM) and 2928 (FSAM) water molecules in FF-MD. The bottom carbon atom of each hydrocarbon (the one furthest away from the water slab) is restrained to be on a hexagonal close-packed lattice with experimental lattice constant $a = 4.69$Å for HSAMs and 5.9Å for FSAMs.[35–37] Box sizes are chosen to be commensurate with the

hexagonal lattice. For FF-MD simulations the restraint is achieved by constraining the position of every one of the bottom carbon atoms individually by a harmonic potential with spring constant $k = 1000$ kJmol^{-1}nm^{-2}. In case of DFT-MD simulations the relative distances between all neighboring bottom carbon atoms are restrained with a harmonic potential of the same spring constant. DFT-MD-simulations are conducted in the NpT ensemble. A constant force is applied to every of the bottom carbon atoms mimicking a piston with 1 bar pressure. At the opposite side of the box a repulsive potential with the distance dependence $(z - z_0)^{-10}$ is applied, which served as a solid wall to the piston. After 10 ps of equilibration, production runs have a duration of 100 ps each.

FF-MD simulations are equilibrated in the NpT ensemble employing a Berendsen barostat with 1 ps time constant and the position of the restraint position is scaled in order to achieve 1 bar pressure in the water phase. Afterwards production runs of 10 ns are conducted in the NVT ensemble.

References

[1] H. Klauk, "Organic thin-film transistors," *Chemical Society Reviews*, vol. 39, no. 7, pp. 2643–2666, 2010.

[2] R. Jin, "Quantum sized, thiolate-protected gold nanoclusters," *Nanoscale*, vol. 2, no. 3, pp. 343–362, 2010.

[3] H. Häkkinen, "The gold-sulfur interface at the nanoscale," *Nature Chemistry*, vol. 4, no. 6, pp. 443–455, 2012.

[4] D. Xiang, X. Wang, C. Jia, T. Lee, and X. Guo, "Molecular-Scale Electronics: From Concept to Function," *Chemical Reviews*, vol. 116, no. 7, pp. 4318–4440, 2016.

[5] U. Srinivasan, M. R. Houston, R. T. Howe, and R. Maboudian, "Alkyltrichlorosilane-based self-assembled monolayer films for stiction reduction in silicon micromachines," *Journal of Microelectromechanical Systems*, vol. 7, no. 2, pp. 252–260, 1998.

[6] E. Hoque, J. A. Derose, P. Hoffmann, B. Bhushan, and H. J. Mathieu, "Chemical stability of nonwetting, low adhesion self-assembled monolayer films formed by perfluoroalkylsilanization of copper," *Journal of Chemical Physics*, vol. 126, no. 11, 2007.

[7] S. P. Pujari, E. Spruijt, M. A. Cohen Stuart, C. J. Van Rijn, J. M. Paulusse, and H. Zuilhof, "Ultralow adhesion and friction of fluoro-hydro alkyne-derived self-assembled monolayers on H-terminated Si(111)," *Langmuir*, vol. 28, no. 51, pp. 17690–17700, 2012.

[8] M. Graupe, M. Takenaga, T. Koini, R. Colorado, and T. R. Lee, "Oriented surface dipoles strongly influence interfacial wettabilities [3]," *Journal of the American Chemical Society*, vol. 121, no. 13, pp. 3222–3223, 1999.

[9] R. Colorado and T. R. Lee, "Wettabilities of self-assembled monolayers on gold generated from progressively fluorinated alkanethiols," *Langmuir*, vol. 19, no. 8, pp. 3288–3296, 2003.

[10] Y. X. Zhuang, O. Hansen, T. Knieling, C. Wang, P. Rombach, W. Lang, W. Benecke, M. Kehlenbeck, and J. Koblitz, "Thermal stability of vapor phase deposited self-assembled monolayers for MEMS anti-stiction," *Journal of Micromechanics and Microengineering*, vol. 16, no. 11, pp. 2259–2264, 2006.

[11] V. H. Dalvi and P. J. Rossky, "Molecular origins of fluorocarbon hydrophobicity," *Proceedings of the National Academy of Sciences*, vol. 107, no. 31, pp. 13603–13607, 2010.

[12] S. Carlson, M. Becker, F. N. Brünig, K. Ataka, R. Cruz, L. Yu, P. Tang, M. Kanduč, R. Haag, J. Heberle, H. Makki, and R. R. Netz, "Hydrophobicity of Self-Assembled Monolayers of Alkanes: Fluorination, Density, Roughness, and Lennard-Jones Cutoffs," *Langmuir*, vol. 37, no. 47, pp. 13846–13858, 2021.

[13] S. A. Clough, Y. Beers, G. P. Klein, and L. S. Rothman, "Dipole moment of water from Stark measurements of H22O, HDO, and D2O," *The Journal of Chemical Physics*, vol. 2254, no. September, pp. 2254–2259, 1973.

[14] Y. S. Badyal, M. L. Saboungi, D. L. Price, S. D. Shastri, D. R. Haeffner, and A. K. Soper, "Electron distribution in water," *Journal of Chemical Physics*, vol. 112, no. 21, pp. 9206–9208, 2000.

[15] M. C. Goh, J. M. Hicks, K. Kemnitz, G. R. Pinto, K. Bhattacharyya, K. B. Eisenthal, and T. F. Heinz, "Absolute orientation of water molecules at the neat water surface," *Journal of Physical Chemistry*, vol. 92, no. 18, pp. 5074–5075, 1988.

[16] Q. Du, R. Superfine, E. Freysz, and Y. R. Shen, "Vibrational spectroscopy of water at the vapor/water interface," *Physical Review Letters*, vol. 70, no. 15, pp. 2313–2316, 1993.

[17] I. V. Stiopkin, C. Weeraman, P. A. Pieniazek, F. Y. Shalhout, J. L. Skinner, and A. V. Benderskii, "Hydrogen bonding at the water surface revealed by isotopic dilution spectroscopy," *Nature*, vol. 474, no. 7350, pp. 192–195, 2011.

[18] L. F. Scatena, M. G. Brown, and G. L. Richmond, "Water at hydrophobic surfaces: Weak hydrogen bonding and strong orientation effects," *Science*, vol. 292, no. 5518, pp. 908–912, 2001.

[19] J. Tomlinson-Phillips, J. Davis, D. Ben-Amotz, D. Spångberg, L. Pejov, and K. Hermansson, "Structure and dynamics of water dangling OH bonds in hydrophobic hydration shells. Comparison of simulation and experiment," *Journal of Physical Chemistry A*, vol. 115, no. 23, pp. 6177–6183, 2011.

[20] P. N. Perera, K. R. Fega, C. Lawrence, E. J. Sundstrom, J. Tomlinson-Phillips, and D. Ben-Amotz, "Observation of water dangling OH bonds around dissolved nonpolar groups," *Proceedings of the National Academy of Sciences of the United States of America*, vol. 106, no. 30, pp. 12230–12234, 2009.

[21] N. Smolentsev, W. J. Smit, H. J. Bakker, and S. Roke, "The interfacial structure of water droplets in a hydrophobic liquid," *Nature Communications*, vol. 8, no. May, pp. 1–6, 2017.

[22] E. K. Watkins and W. L. Jorgensen, "Perfluoroalkanes: Conformational Analysis and Liquid-State Properties from ab Initio and Monte Carlo Calculations," *Journal of Physical Chemistry A*, vol. 105, no. 16, pp. 4118–4125, 2001.

[23] C. Sendner, D. Horinek, L. Bocquet, and R. R. Netz, "Interfacial water at hydrophobic and hydrophilic surfaces: Slip, viscosity, and diffusion," *Langmuir*, vol. 25, no. 18, pp. 10768–10781, 2009.

[24] A. Luzar and D. Chandler, "Hydrogen-bond kinetics in liquid water," *Nature*, vol. 379, pp. 55–57, 1996.

[25] S. Sun, F. Tang, S. Imoto, D. R. Moberg, T. Ohto, F. Paesani, M. Bonn, E. H. Backus, and Y. Nagata, "Orientational Distribution of Free O-H Groups of Interfacial Water is Exponential," *Physical Review Letters*, vol. 121, no. 24, p. 246101, 2018.

[26] F. Tang, T. Ohto, T. Hasegawa, W. J. Xie, L. Xu, M. Bonn, and Y. Nagata, "Definition of Free O-H Groups of Water at the Air-Water Interface," *Journal of Chemical Theory and Computation*, vol. 14, no. 1, pp. 357–364, 2018.

[27] S. Carlson, F. N. Brünig, P. Loche, D. J. Bonthuis, and R. R. Netz, "Exploring the Absorption Spectrum of Simulated Water from MHz to Infrared," *Journal of Physical Chemistry A*, vol. 124, no. 27, pp. 5599–5605, 2020.

[28] F. N. Brünig, O. Geburtig, A. V. Canal, J. Kappler, and R. R. Netz, "Time-Dependent Friction Effects on Vibrational Infrared Frequencies and Line Shapes of Liquid Water," *Journal of Physical Chemistry B*, vol. 126, no. 7, pp. 1579–1589, 2022.

[29] J. R. Robalo, L. M. Streacker, D. Mendes De Oliveira, P. Imhof, D. Ben-Amotz, and A. V. Verde, "Hydrophobic but Water-Friendly: Favorable Water-Perfluoromethyl Interactions Promote Hydration Shell Defects," *Journal of the American Chemical Society*, vol. 141, no. 40, 2019.

[30] J. Hutter, M. Iannuzzi, F. Schiffmann, and J. Vandevondele, "Cp2k: Atomistic simulations of condensed matter systems," *Wiley Interdisciplinary Reviews: Computational Molecular Science*, vol. 4, no. 1, pp. 15–25, 2014.

[31] S. Grimme, J. Antony, S. Ehrlich, and H. Krieg, "A consistent and accurate ab initio parametrization of density functional dispersion correction (DFT-D) for the 94 elements H-Pu," *Journal of Chemical Physics*, vol. 132, no. 15, 2010.

[32] J. VandeVondele and J. Hutter, "Gaussian basis sets for accurate calculations on molecular systems in gas and condensed phases," *Journal of Chemical Physics*, vol. 127, no. 11, 2007.

[33] S. Pronk, S. Páll, R. Schulz, P. Larsson, P. Bjelkmar, R. Apostolov, M. R. Shirts, J. C. Smith, P. M. Kasson, D. Van Der Spoel, B. Hess, and E. Lindahl, "GROMACS 4.5: A high-throughput and highly parallel open source molecular simulation toolkit," *Bioinformatics*, vol. 29, no. 7, pp. 845–854, 2013.

[34] W. L. Jorgensen, D. S. Maxwell, and J. Tirado-Rives, "Development and testing of the OPLS all-atom force field on conformational energetics and properties of organic liquids," *Journal of the American Chemical Society*, vol. 118, no. 45, pp. 11225–11236, 1996.

[35] C. E. Chidsey and D. N. Loiacono, "Chemical Functionality in Self-Assembled Monolayers: Structural and Electrochemical Properties," *Langmuir*, vol. 6, no. 3, pp. 682–691, 1990.

[36] G. Y. Liu, P. Fenter, C. E. Chidsey, D. F. Ogletree, P. Eisenberger, and M. Salmeron, "An unexpected packing of fluorinated n-alkane thiols on Au(111): A combined atomic force microscopy and x-ray diffraction study," *The Journal of Chemical Physics*, vol. 101, no. 5, pp. 4301–4306, 1994.

[37] C. A. Alves and M. D. Porter, "Atomic Force Microscopic Characterization of a Fluorinated Alkanethiolate Monolayer at Gold and Correlations to Electrochemical and Infrared Reflection Spectroscopic Structural Descriptions," *Langmuir*, vol. 9, no. 12, pp. 3507–3512, 1993.

A Appendix

A.1 Infrared absorption spectra from linear response theory

We consider the response of an observable A to a force $h(t)$ which couples to the observable B. The time dependent response of the observable $A(t) = A_0 + \Delta A(t)$ is to first order governed by the linear response relation

$$\Delta A(t) = \int_{-\infty}^{t} \mathrm{d}t' \chi_{AB}(t - t') h(t') + \dots \tag{11}$$

The linear response function χ_{AB} is related to the correlation function $C_{AB} = \langle A(0)B(t)\rangle$ via the fluctuation dissipation relation

$$\chi_{AB} = -\frac{1}{k_B T}\frac{\mathrm{d}}{\mathrm{d}t}C_{AB}(t)\,. \tag{12}$$

In order to satisfy causality, $\chi(t)$ has to be single-sided, i.e. $\chi(t) = 0$ for $t < 0$. Fourier transforming Eq. 12 we find

$$\tilde{\chi}_{AB}(\omega) = -\frac{1}{k_\mathrm{B} T}\int_{\infty}^{\infty} \mathrm{d}t\; e^{i\omega t}\frac{\mathrm{d}}{\mathrm{d}t}C_{AB}(t) \tag{13}$$

$$\tilde{\chi}_{AB}(\omega) = -\frac{1}{k_\mathrm{B} T}\left(C_{AB}(0) - i\omega\int_{0}^{\infty} \mathrm{d}t\; e^{i\omega t}C_{AB}(t)\right) \tag{14}$$

The dielectric susceptibility $\tilde{\chi}$ is the linear response of a systems polarization to an applied electric field. Therefore, it is given by

$$\tilde{\chi}(\omega) = -\frac{1}{k_\mathrm{B} T}\left(C_{\mathbf{MM}}(0) - i\omega\int_{0}^{\infty} \mathrm{d}t\; e^{i\omega t}C_{\mathbf{MM}}(t)\right) \tag{15}$$

with polarization-autocorrelation function $C_{\mathbf{MM}}(t)$. Realizing that autocorrelation functions are real and symmetric, the imaginary part of the dielectric response function follows to be

$$\tilde{\chi}''(\omega) = \frac{1}{k_B T}\omega\mathrm{Re}\left[C_{AB}(0) - i\omega\int_{0}^{\infty} \mathrm{d}t\; e^{i\omega t}C_{AB}(t)\right] \tag{16}$$

$$= \frac{\omega}{2k_B T}\tilde{C}_{\mathrm{MM}}(\omega)\,. \tag{17}$$

Here, we use the Wiener-Khinchin theorem to compute the autocorrelation function of M for the finite time interval $[0, t_{\max}]$ in the frequency domain. For the dielectric power spectrum we use

$$\omega\tilde{\chi}''(\omega) = \frac{\omega^2}{2k_B T t_{\max}}|\tilde{\mathrm{M}}(\omega)|^2\,. \tag{18}$$

A.2 Approximation of the absorption spectra from positional data

In the main text we analyze the contribution of dangling OH bonds to the infrared absorption spectrum in terms of power spectra of the OH bond length. The total dipole moment of the considered system can be written in terms of molecular dipole moments

$$\mathbf{M}(t) = \sum_{i=1}^{n_{\mathrm{mols}}}\mathbf{M}_i(t) \tag{19}$$

which leads to a decomposition of the dielectric spectrum into a molecular and collective contribution

$$C_{\mathbf{MM}}(t) = \left\langle\sum_i \mathbf{M}_i(0)\cdot\sum_i \mathbf{M}_i(t)\right\rangle = \sum_i\langle\mathbf{M}_i(0)\mathbf{M}_i(t)\rangle + \sum_{i\neq j}\langle\mathbf{M}_i(0)\mathbf{M}_j(t)\rangle \tag{20}$$

Both the collective and the molecular part contribute roughly equal to the OH - stretch peak.[27] As the name says it is commonly assumed that the OH - stretch peak is caused by a stretching movement of the OH-bond length. To estimate the contribution of this coordinate to the total IR-absorption spectrum we expand the dipole moment of a single water molecule with respect to the internal OH vectors $\mathbf{r}_{\mathrm{OH}}$.

$$\mathbf{M}(\mathbf{r}_{\mathrm{OH},1}, \mathbf{r}_{\mathrm{OH},2}) = \mathbf{M}_0 + \mu(\mathbf{r}_{\mathrm{OH},1} + \mathbf{r}_{\mathrm{OH},2}) + \nu\mathbf{r}_{\mathrm{OH},1}\cdot\mathbf{r}_{\mathrm{OH},2}(\mathbf{r}_{\mathrm{OH},1} + \mathbf{r}_{\mathrm{OH},2}) + \dots\,. \tag{21}$$

The first term includes a base dipole moment along all influences including out-of-plane contributions from surrounding water molecules. The second term is linear in the OH-distance and will be studied here. The third term which is the first mixed one in the expansion gives alongside other cross contributions the bending contribution. In order to verify that the dipole moment can be approximated to be linear in the OH-distance we calculate projection of the dipole moment on the OH vector. In Fig. 5 we show this projection as function of the OH distance for water molecules in the bulk phase as well as for a single water molecules in the vapor phase. In vapor phase there is a clear linear dependence. For bulk phase water molecules the average of the dipole moment still shows good agreement with the linear least square fit of the data, but it is apparent that this linear approximation does not coincide with the principal component axis of the displayed data. This means there is some underlying coupling in the system which is not perfectly captured by the OH distance coordinate.

Assuming a linear dependence of the dipole moment on the OH distance it follows that the infrared absorption is proportional to the power spectrum of the OH bond distance

$$\omega\chi''(\omega) \propto \frac{\omega^2}{2k_B T t_{\max}}|\tilde{d}(\omega)|^2 \tag{22}$$

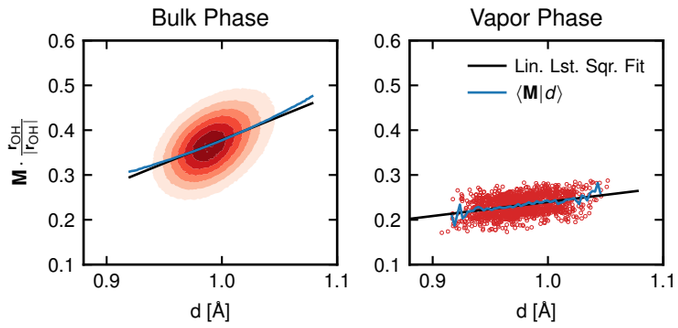

Figure 5: Dipole moment of a water molecule as a function of its OH bond distance.

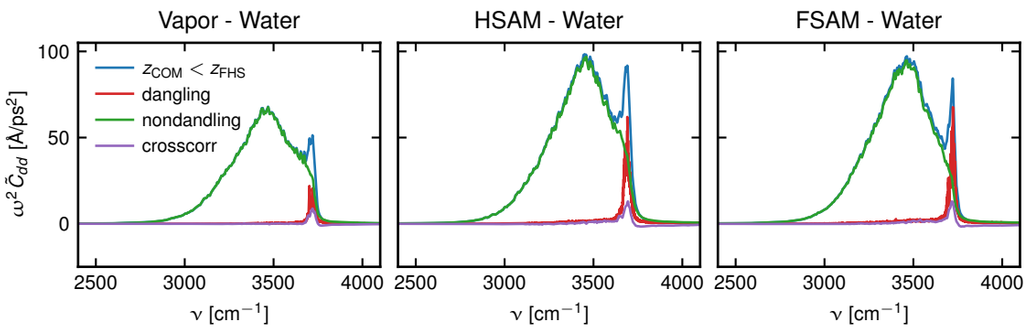

Figure 6: Decomposition of the velocity autocorrelation spectrum of OH distances of water molecules in the first hydration layer into dangling, nondangling and crosscorrelation contributions.

A.3 Decomposition of the OH spectrum into contributions from different water structures

For every OH bond we get a time series $d(t)$ which is contributing to the molecular part of the infrared absorption spectrum. At time t a bond can either be in a dangling or nondangling configuration. Therefore, the trajectory can be partitioned into dangling and nondangling subparts

$$d^{\mathrm{d/nd}}(t) = \begin{cases} d^{\mathrm{d/nd}}(t) = d(t) & \text{if bond is dangling / nondangling} \\ 0 & \text{otherwise .} \end{cases} \tag{23}$$

Clearly, this partitioning is additive and the OH distance autocorrelation function $C_{dd}(t)$ can be partitioned analogously to Eq. 20 into a contribution of all the dangling and all the nondangling configurations plus a cross term

$$C_{dd}(\tau) = \underbrace{\langle d^{\mathrm{d}}(t) d^{\mathrm{d}}(t+\tau)\rangle}_{\text{dangling}} + \underbrace{\langle d^{\mathrm{nd}}(t) d^{\mathrm{nd}}(t+\tau)\rangle}_{\text{nondangling}} + \underbrace{\langle d^{\mathrm{d}}(t) d^{\mathrm{nd}}(t+\tau)\rangle}_{\text{cross}}, \tag{24}$$

In Fig. 6 we show the partitioning of C_{dd} for water molecules in the first hydration layer of different interfaces. The cross terms give only small contributions in the dangling regime which is an indicator for a good criterion. We used the criteria for dangling OH bonds which are described in the main text and further discussed in the appendix in Sec. A.4.

A.4 Criteria for dangling OH bonds

We developed a criterion for dangling OH bonds based on the splitting of of the vibrational signature which was explained in the preceding section of the appendix. The criterion is based on the center of mass position of the water molecule of the OH bond z_{COM} and the angle the bond forms with the normal vector of the considered interface θ_{OH}. We scan the parameter space of (z_{COM}, θ_{OH}) and calculate the dangling part of the OH vibrational spectrum. An optimal criterion would yield a spectrum with maximal amplitude around the dangling frequency around 3700 cm^{-1} while at the meantime minimizing contributions in the bulk OH regime. The dangling spectral contributions are displayed in Fig. 7. In case of SAM – water interfaces we found the best combination to be ($z_{\mathrm{COM}} = z_{\mathrm{GDS}} + 1.0$Å, $\theta_{\mathrm{OH}} = 120°$). At the same distance at the vapor – water interface one can see substantial contributions of hydrogen bonded OH bonds. We assume this to be because of fluctuations of the instantaneous interfacial positions. Thus, we choose a more restrictive distance of $z_{\mathrm{COM}} = z_{\mathrm{GDS}} + 0.0$Å in case of the vapor–water interface.

A.5 Fitting of dangling water vibrational properties

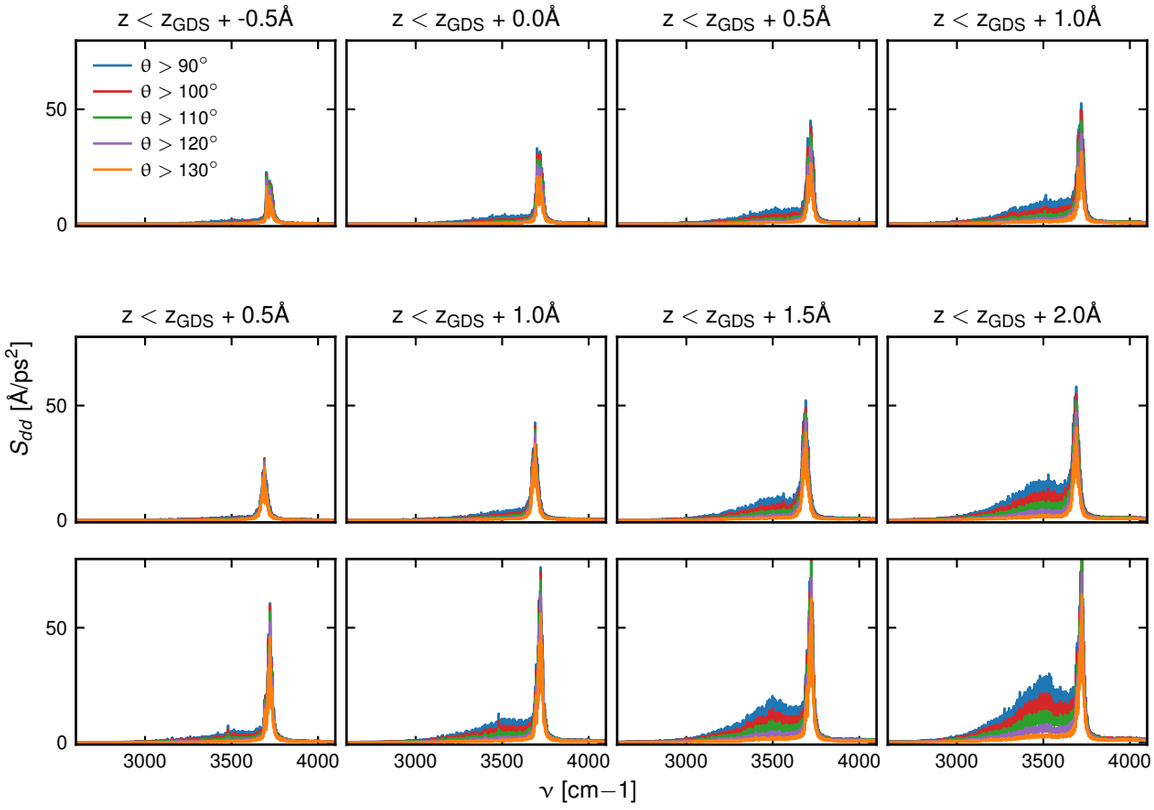

Figure 7: Contribution of dangling OH-bonds to the velocity autocorrelation spectrum of the first hydration layer for different criteria for dangling bonds. 1st row vapor-water, 2nd row HSAM-water, 3rd row FSAM water system.

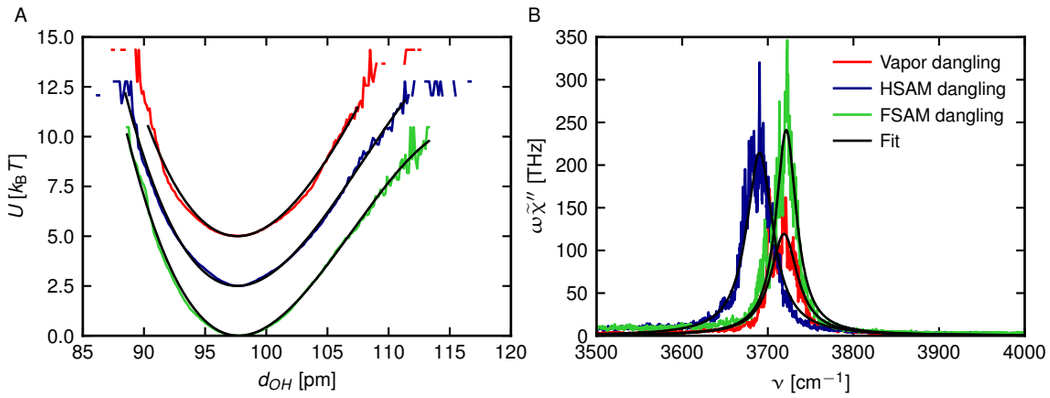

Figure 8: Fits of dangling OH bonds properties. A: colored lines show the effective potential of dangling OH bond length which were also shown in Fig. 4 of the main text. Black lines show fits according to Eq. 9 of the main text. B: Dangling contributions to the velocity autocorrelation spectrum of OH bond distances of water molecules in the first hydration layer. Black lines denote fits according to the Lorentzian line shape from Eq. 7 of the main text.